True logarithmic amplification of frequency clock in SS-OCT for calibration

Bin Liu,[1,2] Ehsan Azimi,[1,2] and Mark E. Brezinski[1,2*]

[1]*Department of Orthopedic Surgery, Brigham and Women's Hospital, 75 Francis Street, Boston, MA 02115, USA*
[2]*Harvard Medical School, 25 Shattuck Street, Boston, MA 02115, USA*
**mebrezin@mit.edu*

Abstract: With swept source optical coherence tomography (SS-OCT), imprecise signal calibration prevents optimal imaging of biological tissues such as coronary artery. This work demonstrates an approach using a true logarithmic amplifier to precondition the clock signal, with the effort to minimize the noises and phase errors for optimal calibration. This method was validated and tested with a high-speed SS-OCT. The experimental results manifest its superior ability on optimization of the calibration and improvement of the imaging performance. Particularly, this hardware-based approach is suitable for real-time calibration in a high-speed system where computation time is constrained.

OCIS codes: (170.4500) Optical coherence tomography; (120.3180) Interferometry.

References and links

1. M. E. Brezinski, *Optical Coherence Tomography: Principle and Practice* (Academic, Burlington, 2006).
2. M. E. Brezinski and J. G. Fujimoto, "Optical coherence tomography: high-resolution imaging in nontransparent tissue," IEEE J. Sel. Top. Quantum Electron. **5**(4), 1185–1192 (1999).
3. M. E. Brezinski, G. J. Tearney, B. E. Bouma, J. A. Izatt, M. R. Hee, E. A. Swanson, J. F. Southern, and J. G. Fujimoto, "Optical coherence tomography for optical biopsy. Properties and demonstration of vascular pathology," Circulation **93**(6), 1206–1213 (1996).
4. G. J. Tearney, M. E. Brezinski, B. E. Bouma, S. A. Boppart, C. Pitris, J. F. Southern, and J. G. Fujimoto, "In vivo endoscopic optical biopsy with optical coherence tomography," Science **276**(5321), 2037–2039 (1997).
5. D. Huang, E. A. Swanson, C. P. Lin, J. S. Schuman, W. G. Stinson, W. Chang, M. R. Hee, T. Flotte, K. Gregory, C. A. Puliafito, and J. G. Fujimoto, "Optical coherence tomography," Science **254**(5035), 1178–1181 (1991).
6. G. J. Tearney, B. E. Bouma, and J. G. Fujimoto, "High-speed phase- and group-delay scanning with a grating-based phase control delay line," Opt. Lett. **22**(23), 1811–1813 (1997).
7. S. R. Chinn, E. A. Swanson, and J. G. Fujimoto, "Optical coherence tomography using a frequency-tunable optical source," Opt. Lett. **22**(5), 340–342 (1997).
8. A. F. Fercher, C. K. Hitzenberger, G. Kamp, and S. Y. Elzaiat, "Measurement of intraocular distances by backscattering spectral interferometry," Opt. Commun. **117**(1-2), 43–48 (1995).
9. M. Gora, K. Karnowski, M. Szkulmowski, B. J. Kaluzny, R. Huber, A. Kowalczyk, and M. Wojtkowski, "Ultra high-speed swept source OCT imaging of the anterior segment of human eye at 200 kHz with adjustable imaging range," Opt. Express **17**(17), 14880–14894 (2009).
10. R. Huber, M. Wojtkowski, and J. G. Fujimoto, "Fourier domain mode locking (FDML): a new laser operating regime and applications for optical coherence tomography," Opt. Express **14**(8), 3225–3237 (2006).
11. S. Moon and D. Y. Kim, "Ultra-high-speed optical coherence tomography with a stretched pulse supercontinuum source," Opt. Express **14**(24), 11575–11584 (2006).
12. W. Y. Oh, S. H. Yun, G. J. Tearney, and B. E. Bouma, "115 kHz tuning repetition rate ultrahigh-speed wavelength-swept semiconductor laser," Opt. Lett. **30**(23), 3159–3161 (2005).
13. C. M. Eigenwillig, B. R. Biedermann, G. Palte, and R. Huber, "K-space linear Fourier domain mode locked laser and applications for optical coherence tomography," Opt. Express **16**(12), 8916–8937 (2008).
14. A. H. Cordes, G. B. Xavier, G. Vilela de Faria, and J. P. von der Weid, "High axial resolution swept source for optical coherence tomography," Electron. Lett. **46**(1), 27–28 (2010).
15. U. Glombitza and E. Brinkmeyer, "Coherent frequency-domain reflectometry for characterization of single-mode integrated-optical wave-guides," J. Lightwave Technol. **11**(8), 1377–1384 (1993).
16. E. Brinkmeyer and R. Ulrich, "High-resolution OCDR in dispersive wave-guides," Electron. Lett. **26**(6), 413–414 (1990).
17. E. Azimi, B. Liu, and M. E. Brezinski, "Real-time and high-performance calibration method for high-speed swept-source optical coherence tomography," J. Biomed. Opt. **15**(1), 016005 (2010).
18. T. Wu, Z. H. Ding, K. Wang, and C. Wang, "Swept source optical coherence tomography based on non-uniform discrete fourier transform," Chin. Opt. Lett. **7**(10), 941–944 (2009).

#140944 - $15.00 USD Received 19 Jan 2011; revised 9 May 2011; accepted 25 May 2011; pub. 27 May 2011

19. B. J. Vakoc, S. H. Yun, J. F. de Boer, G. J. Tearney, and B. E. Bouma, "Phase-resolved optical frequency domain imaging," Opt. Express **13**(14), 5483–5493 (2005).
20. S. H. Yun, G. J. Tearney, B. E. Bouma, B. H. Park, and J. F. de Boer, "High-speed spectral-domain optical coherence tomography at 1.3 μm wavelength," Opt. Express **11**(26), 3598–3604 (2003).
21. R. Huber, M. Wojtkowski, K. Taira, J. G. Fujimoto, and K. Hsu, "Amplified, frequency swept lasers for frequency domain reflectometry and OCT imaging: design and scaling principles," Opt. Express **13**(9), 3513–3528 (2005).
22. J. Zhang, J. S. Nelson, and Z. P. Chen, "Removal of a mirror image and enhancement of the signal-to-noise ratio in Fourier-domain optical coherence tomography using an electro-optic phase modulator," Opt. Lett. **30**(2), 147–149 (2005).
23. R. Huber, M. Wojtkowski, J. G. Fujimoto, J. Y. Jiang, and A. E. Cable, "Three-dimensional and C-mode OCT imaging with a compact, frequency swept laser source at 1300 nm," Opt. Express **13**(26), 10523–10538 (2005).
24. D. C. Adler, Y. Chen, R. Huber, J. Schmitt, J. Connolly, and J. G. Fujimoto, "Three-dimensional endomicroscopy using optical coherence tomography," Nat. Photonics **1**(12), 709–716 (2007).
25. J. Xi, L. Huo, J. Li, and X. Li, "Generic real-time uniform K-space sampling method for high-speed swept-source optical coherence tomography," Opt. Express **18**(9), 9511–9517 (2010).
26. C. H. Chen, "Signal-to-noise ratios in logarithmic amplifiers," Proc. IEEE **57**, 1167–1168 (1969).
27. B. Liu, E. Azimi, and M. E. Brezinski, "Improvement in dynamic range limitation of swept source optical coherence tomography by true logarithmic amplification," J. Opt. Soc. Am. A **27**(3), 404–414 (2010).

1. Introduction

Optical coherence tomography (OCT) measures the depth-resolved backreflections from a biological tissue with up to sub-micron-level resolution, and can perform imaging at or above the video rate. These unique capabilities have granted OCT numerous applications in medicine and biology [1–4]. Early OCT systems were commonly built on the low coherence interferometry by altering the optical path length in the reference arm of an interferometer and measuring the interferogram in the time domain, which is thus referred to as the time domain OCT (TD-OCT) [5,6]. Recently, swept source OCT (SS-OCT) has attracted a considerable attention, in which the interferogram is generated by tuning the optical frequency f, or equivalently the wavenumber k of a near-monochromatic light source, usually a tunable laser, while the optical path length in the reference arm remains fixed. Therefore, the interferogram is a function of f or k, although it is measured time-sequentially by a photo detector. Through inverse Fourier transform, the axial backreflection profile of the sample (the A-scan of OCT) that is actually encoded in such a spectral interferogram can be recovered as a function of time delay τ or axial distance z [7,8]. This approach can drastically alleviate the complexity of the scan mechanics used in TD-OCT, and has demonstrated extremely high imaging speed without any mechanical movement in the reference arm [9–12].

For the A-scan recovering, discrete Fourier transform (DFT) or fast Fourier transform (FFT) is practically performed on a digitized interferogram. Commonly the interferogram is sampled with equal temporal intervals by an analog-to-digital (A/D) converter, which means the data set is evenly distributed in time domain but not necessarily in the frequency or wavenumber domain. Unless the frequency/wavenumber is tuned linearly with time [13,14], direct FFT on this data set which is non-equidistantly distributed in the f or k domain, will introduce significant transform errors. These errors may dramatically compromise the performance of a SS-OCT such as its axial resolution and signal to noise ratio (*SNR*) [9,15–17]. Unfortunately, in many SS-COT systems, the relationship between the tuned frequency/wavenumber and the time is not linear due to the tuning mechanism of a source. Therefore, the digitized interferogram has to be remapped into and evenly distributed in the frequency/wavenumber domain before conducting FFT, which has become a standard calibration procedure in SS-OCT signal processing. If the f vs. t relationship can maintain highly stable and repeatable *inter* scans. This relationship just need to be determined *a priori*, then can be repeatedly used for calibration. However, few SS-OCT systems can do that. On the contrary, the stability and repeatability of the frequency scanning in many systems are always compromised, particularly when the light source scans at a fast rate. In these cases, the accordance between f and t needs to be measured in real time. Although an alternative in terms of non-uniform DFT has been introduced with no need of calibration [18], the f vs. t relationship still needs to be measured for determining the varied DFT bins, and the computation time is presumably increased.

#140944 - $15.00 USD Received 19 Jan 2011; revised 9 May 2011; accepted 25 May 2011; pub. 27 May 2011

Popularly, the calibration procedure in SS-OCT employs a frequency clock, which is capable of providing a form of *f* vs. *t* relationship while the frequency of the source is scanning. A variety of frequency clocks have been used in literature, such as a narrowband filter, a Fabry–Perot (FP) interferometer, equivalently an optical etalon, or a Mach-Zehnder interferometer (MZI) with uneven optical path lengths between two arms. A narrowband filter can pick out a specific frequency line as a checking point when the source is scanning [19,20]. However, this method can only dynamically compensate the instability of the starting frequency, but requires high repeatability of the scanned spectrum. The F-P clock [21,22], and the MZI clock [23] shares the same principle of calibration: A small portion of the source output is guided into an auxiliary interferometer. While the source is scanning, an interferogram is generated, and can be picked up by a photo detector, which is referred to as the frequency clock signal. Usually the clock signal is sent to an A/D converter and digitized with OCT signal synchronously but separately. The F-P interferogram is a series of pulses, which are equally distanced in frequency/wavenumber domain, and the difference between adjacent maxima is determined by the free spectral range (FSR) of the interferometer. Once the positions of these maxima are determined in the sampled clock data set, the corresponding samples in OCT data set can therefore be singled out, which are equal-spaced in the frequency domain with certain accuracy. The clock signal from a MZI has a sinusoidal waveform, in which adjacent extrema (peaks, troughs,) or points crossing DC offset are equally spaced in the frequency/wavenumber space. Using MZI clock may provide some prominent advantages over F-P clock: 1) Crossing points can be referenced as well. Together with those extrema, a MZI clock provides twice more reference points than an F-P clock with the same FSR. 2) The balanced detection technique can be used to reduce phase error/noise in the clock signal.

Finding the extrema and crossing points in a MZI clock signal can be done either with software or with hardware-based approaches. Several hardware-based approaches have been reported to extract the trigger signal from the MZI clock for A/D conversion. Therefore, the A/D converter can sample the OCT signal uniformly in the *f*/*k* domain and they also do not need redundant sampling [24,25]. However, the triggering locations are substantially sensitive to noises in the MZI clock, and generated errors may not be easily corrected. More commonly, searching extrema and crossings is done by software after the signal digitization, which is more flexible to clock settings and advanced algorithms, but needs a second A/D channel and computation. A nearest neighbor check algorithm is popularly used in current SS-OCT systems for calibration [21]. Its basic concept is using a sliding window with fixed width (e.g., 3 points or 5 points) to select consecutive subset in the clock data set, and then search any extrema within this subset as final finding. This algorithm needs less computation and is presumably fast for calibration. However, its accuracy is substantially compromised as its intrinsic sensitivity to noises or phase errors in the clock signal. Our previous work demonstrated a real-time calibration algorithm based on a genetic algorithm, through which the calibration accuracy was significantly improved in SS-OCT [17]. However, practically, the prominent noise cannot be easily and completely eliminated in the clock signal, which may substantially affect the calibration accuracy. In addition, the advanced calibration is done within the software, which inevitably increases the computer processing burden.

The work presented here introduces an approach by preconditioning of clock signal using true logarithmic amplification (TLA), in an effort to reduce noises or phase errors in the clock signal. This approach was validated and tested with a high-speed SS-OCT system, adapted from a commercial system. The experimental results demonstrate that, even with conventional calibration algorithm, the performance of the SS-OCT was improved substantially in terms of the axial resolution and the *SNR* at its full imaging range. Without adding any burden to the computation, this hardware-based approach can effectively optimize the calibration procedure, and hence improve the imaging performance of a SS-OCT system. This method is specifically suitable for a high-speed system, which has constrains on the computation time.

#140944 - $15.00 USD Received 19 Jan 2011; revised 9 May 2011; accepted 25 May 2011; pub. 27 May 2011

2. Methods

The method for improving the calibration accuracy in SS-OCT was validated and tested with a high-speed SS-OCT, which was modified from a commercial SS-OCT system (OCM-1300SS, Thorlabs, Newton, NJ.) The general optical and electronic arrangement is depicted as Fig. 1. A fiber optic Michelson interferometer played the core architecture. The swept laser source (SL1325-P16, Thorlabs, Newton, NJ) provided ~100nm wavelength scan range around 1325 nm central wavelength, as well as above 10 mW output power. The nominal value of the instantaneous coherence length of the source was about 7mm, which was determined by the instantaneous linewidth of the source. The wavelength sweeping rate was 16 kHz. In this the source, an auxiliary MZI was embedded to provide a frequency clock with 100GHz FSR. The interferograms/OCT signal from the Michelson interferometer was detected by a dual-balanced detector (PDB-145C, Thorlabs, Newton, NJ). In the reference arm, a motorized Lefevre type polarization controller was built and implemented for polarization maneuver. The sample beam was scanned by an X-Y scanner (Cambridge Technology, Cambridge, MA,) and was focused on the sample through an objective lens with 30mm focal length. All of the digital signal processing, image reconstruction, scanning control, and system synchronization control was conducted through a high performance personal computer, which was equipped with a high-speed 14-bit A/D card with two channel analog inputs, and 125 MS/s sampling rate (ATS-460, Alazar Tech, Pointe-Claire, Canada). A 16-bit, 4- channel, 1MS/s D/A converter (NI-6731, National Instrument, Austin, TX) was used to generate control signals.

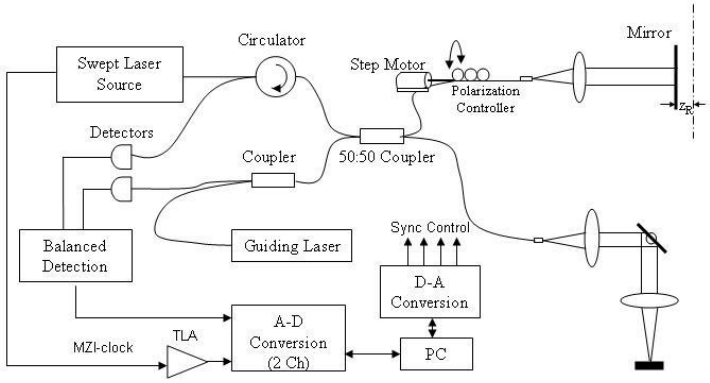

Fig. 1. Schematics of the SS-OCT with a TLA implemented in the clock channel.

The key modification in the setup was that, the MZI clock signal was not directly sent to the A/D card as usual. Instead, it was first sent to a true logarithmic amplifier (Analog Module Inc, AMI-384, Longwood, FL), and then routed to the A/D card as shown in Fig. 1. The TLA can provide about 90dB nominal dynamic range, and a DC-30MHz operating bandwidth. The TLA converts the clock signal from the linear scale to the logarithmic scale before digitization. In a typical TLA, the relationship between the output and input signal with presence of noise can be expressed as [26]

$$s_o + n_o = K \log_{10}\left(\frac{a + s_i + n_i}{\sigma}\right) \quad (1)$$

where s_i and s_o represent the input and output signal respectively. Similarly, in Eq. (1), n_i and n_o represent the noise in the input or output. K is a coefficient in the unit of Volt/dB, and σ is the standard deviation of the noise, presumably a white noise. A bias, a, is usually set in the circuitry to keep the input voltage positive with high probability. Through this nonlinear conversion, signal components with small amplitude are magnified and well preserved, but large amplitude components are compressed. Thus, by true logarithmic amplification, a signal with wide dynamic range can be well preserved through the system, with certain degradation

#140944 - $15.00 USD Received 19 Jan 2011; revised 9 May 2011; accepted 25 May 2011; pub. 27 May 2011

in the resolution of large signals. Our previous work successfully applied this technique for improving the dynamic range of SS-OCT through logarithmic amplification of OCT signal [27].

The relationship between the output *SNR* and the input *SNR* of the TLA can be derived from Eq. (1), but formulated differently for two distinct input conditions. In the case of large input *SNR*, e.g., ≥10, the output *SNR* is approximated as

$$\frac{s_o^2}{\overline{n_o^2}} \approx \frac{s_i^2}{\sigma^2}[\ln(\frac{s_i^2}{\sigma^2})^{\frac{1}{2}}]^2 \tag{2}$$

In the case of small input *SNR*, the output *SNR* equals

$$\frac{s_o^2}{\overline{n_o^2}} = \frac{s_i^2}{\sigma^2}\{\frac{a^2}{\sigma^2}[1+(\frac{s_i^2}{\sigma^2})\frac{1}{2(1+\frac{2a^2}{\sigma^2})}]\} \tag{3}$$

From Eq. (2) and (3), it is observed that TLA improves its output *SNR* at all input *SNR* if the bias is set at or above the level of σ, which is the usual case in a TLA circuitry. Furthermore, there is a substantial improvement of output *SNR* when the input *SNR* becomes large. It is worthwhile to point out that, this model may have some limitations on describing the analog signal computation in a TLA. For example, it does not incorporate necessary processes for noise shaping in the chip such as feedback and filtering. An implication from this insufficient model that digital logarithmic operation could obtain the same calibration results as the TLA might be unrealistic. Careful differentiation will be helpful in practice. Further studies on improved models are needed in the future.

For the application presented here, there are two possible mechanisms can be identified for improving the calibration performance:

1) As indicated by Eq. (2), a log-amplified clock signal has much higher output *SNR* in the regions around the extrema, where the clock signal poses a fairly large input *SNR*. This improvement leads to much fewer fluctuations in the output. This phenomenon can be observed in Fig. 2, where Fig. 2(A1) is a typical MZI clock waveform, and (A2) is its local enlargement, from which the presence of substantial noises can be seen. Figure 2(B1) shows the clock waveform after the TLA, and (B2) gives its local view. It can be seen that, the clock signal with TLA has less fluctuations at its extreme regions, which attributes to the profoundly improved *SNR*. In both local graphs, dot markers represent the sample positions in this digitized clock signal. This example demonstrates that, with TLA in the clock channel, the noise around extreme regions can be dramatically suppressed, which can lead to more precise calibration in SS-OCT and finally improvement in its imaging performance.

2) Figure 2 also demonstrates that, after logarithmic amplification, the edges (rising or falling) of the clock waveform are more abrupt. This outcome suggests that the points of crossing in a logarithmic-amplified clock signal will be less sensitive to phase errors, and are closer to their ideal locations. This can possibly be the second mechanism underlying the designated procedure.

#140944 - $15.00 USD Received 19 Jan 2011; revised 9 May 2011; accepted 25 May 2011; pub. 27 May 2011

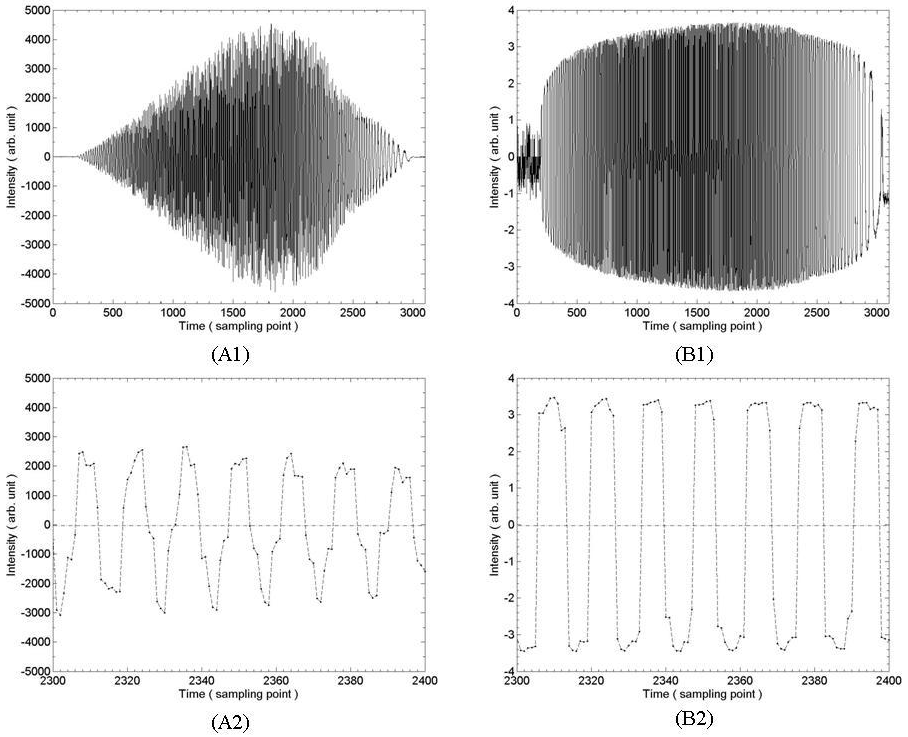

Fig. 2. A typical MZI clock waveform (A1) and its local enlargement (A2). The waveform of the clock after going through the TLA (B1) and its local enlargement (B2).

Through these two mechanisms, the errors and noises in clock signal can be substantially reduced. Thus, the calibration procedure is optimized and its accuracy can be improved. Although bandpass filters has previously been used for preconditioning a linear-scale clock signal [23], hardware or software based bandpass filtering technique might only help a little. Due to the fact that the clock is basically a wideband signal in the order of MHz [17], any matching bandpass filter can only have low Q-value and rule out limited noises. Extra computation might be another drawback for software based approaches. It is also important to be noticed that, due to the excellent pulse response of the TLA (, typically within the range of 10 to 15ns throughout the entire operating bandwidth,) the phase lag introduced by the TLA is subtle, and its influence on the calibration is negligible.

For evaluating the effectiveness of this calibration approach, a reflector was placed at the focal point in the sample arm. The system was set at one-dimensional (A-scan) imaging mode. The sampling rate of the A/D card was set as 50 MS/s. The A/D card's application program interface was used to simultaneously acquire both clock signal and OCT signal in real time, and twelve consecutive OCT signal of the reflector and corresponding clock signal were captured and saved into data files for post-processing. To compare with the calibration procedure with the regular clock, the same measurement process was repeated by bypassing the TLA. Further evaluation at different A-scan depth was also conducted by translating the mirror in the reference arm, with sample reflector position fixed. This arrangement can measure the reflection signal from the reflector, *i.e.*, the point spread function of the system, at different depths while maintaining the light intensity in both arms stable, which is essential for comparison.

Each pair of OCT signal and clock signal traces were post-processed using a program developed with Matlab (Mathworks, Natick, MA.) First, the clock data set was examined by the nearest neighbor check algorithm, to find extrema or crossing points. The OCT data set

#140944 - $15.00 USD Received 19 Jan 2011; revised 9 May 2011; accepted 25 May 2011; pub. 27 May 2011

was indexed by referencing these searched points. Up to this step, the calibration procedure was completed. Then, FFT was conducted on this selected OCT data set and an individual A-scan of the reflector, or equivalently PSF, was retrieved. Quantitative measurement of the full-width-half-maximum (FWHM) of the PSF was obtained. The mean value and standard deviation was also calculated over the 12 consecutive traces. The change on *SNR* was assessed qualitatively. Finally, the average FWHM at each depth was compared between the condition with the logarithmic-amplified clock and the one with the regular clock.

Two-dimensional images of the reflector were captured as well for comparison purpose. The images were acquired through the manufacture's software, in which the calibration algorithm is unknown. Again, the image acquisition and comparison were performed between the condition with logarithmic-amplified clock and the one with regular clock.

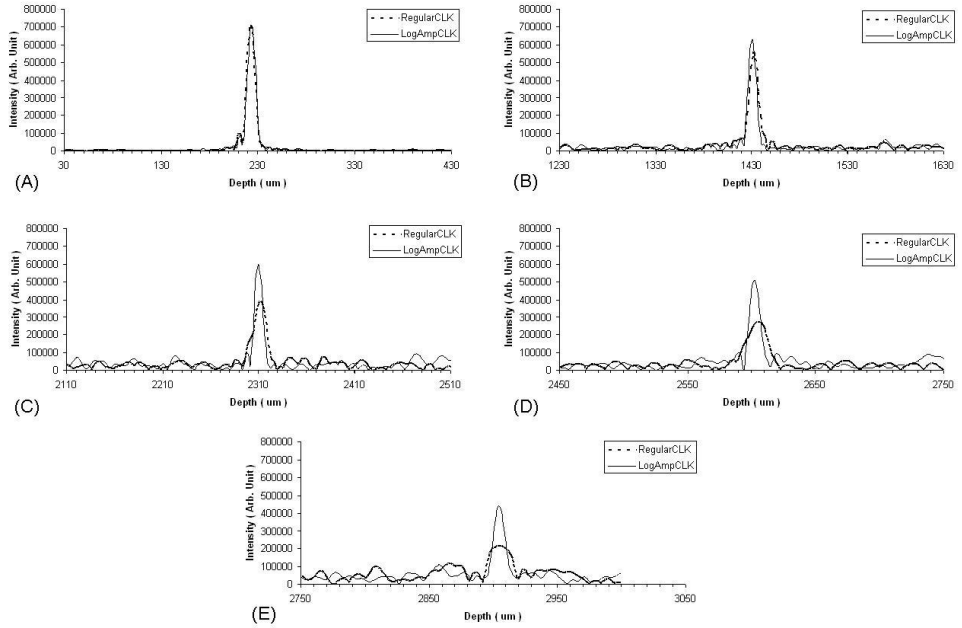

Fig. 3. Sample A-scans of the reflector at different depths, calibrated with log-amplified clock and regular clock respectively.

3. Results and discussion

Figure 3 demonstrates sample A-scans of the reflector at different imaging depths: (A) ~0.22mm, (B) ~1.43mm, (C) ~2.31mm, (D) ~2.60mm, and (E) ~2.90mm. Within each graph, two A-scans are displayed, which were calibrated and retrieved through different optical frequency clock signal: the dash line represents using a regular MZI clock; Solid line represents using a log-amplified MZI clock. Except this only difference, the signal processing for both remains the same. Particularly, the corresponding spectral interferograms for both were calibrated into *k*-space by the same algorithm of searching the extrema in clock signal. Through (A) to (E), a phenomenon, associated with regular MZI clock recalibration, is observed as the point spread function (PSF) rapidly spreads while imaging depth gradually increases. This indicates that the axial resolution at deeper imaging range is inevitably compromised, specifically beyond the half of the total 3mm range. Furthermore, the resolution degradation is accompanied by a rapid signal dropping, which is largely due to the non-optimized calibration where the signal intensity is more dispersed in its Fourier transform domain. On the contrary, by using log-amplified clock signal, PSF signals show little change in terms of shape and width through (A) to (E), which suggests a better and steady axial

#140944 - $15.00 USD Received 19 Jan 2011; revised 9 May 2011; accepted 25 May 2011; pub. 27 May 2011

resolution throughout entire imaging range. The slight and gradual signal roll-off is presumably attributed to the instantaneous linewidth of the source singly, but not the calibration procedure itself. It is observed that the signal drop-off at depth of 2.9mm is about three fifth of the one around 0.23mm, which is within the range of drop-off caused by the instantaneous linewidth of the source, considering that the nominal coherence length of the source is about 7mm (, equivalently 3.5mm in depth.)

Table 1 lists mean values and standard deviations of the FWHM of PSFs, given the calibration algorithm as described in the methods section. PSFs were measured at five discrete imaging depths, *i.e.*, d1≈0.22mm, d2≈1.43mm, d3≈2.31mm, d4≈2.60mm, and d5≈2.90mm. At each depth, 12 PSFs were measured with using the regular clock; another 12 measurements were conducted with using the log-amplified clock. With regular clock, the average FWHM and standard deviation of the FWHMs drastically increases when depth increases. With log-amplified clock, the averages of FWHMs retain a much smaller and constant value around 10.6μm, throughout the whole imaging range. Meanwhile, little variation can be seen in standard deviations. These results demonstrate significant improvements on axial resolution of a SS-OCT by using log-amplified frequency clock for calibration.

Table 1. Average FWHM (mean ± standard deviation) at different depths

	d1≈0.22 mm	d2≈1.43 mm	d3≈2.31 mm	d4≈2.60 mm	d5≈2.90 mm
Regular CLK	10.7 ± 0.1μm	12.0 ± 0.3μm	15.7 ± 0.8μm	18.9 ± 1.8μm	21.0 ± 3.7μm
Log CLK	10.6 ± 0.1μm	10.6 ± 0.2μm	10.5 ± 0.1μm	10.6 ± 0.2μm	10.7 ± 0.5μm

Figure 4 gives sample OCT images of the reflector, at about 2.5mm depth: (A) an image captured by the system with typical factory-configurations, whose resolution is 512x1024pixel (HxW) corresponding to 3x6mm (HxW) view field, and a local enlargement (128x128pixel with the same pixel rate); (B) an image, with the same image specifications as (A), captured by the same system but a true logarithmic amplifier was inserted in the MZI clock channel as described in the methods section. A local extraction and enlargement, from the same area as (A), is displayed as well. The difference in linewidth between the two images is prominent. Comparison between two local enlargements demonstrates that the system with log-amplified clock provides better axial resolution for SS-OCT. It also demonstrates that the TLA approach is versatile to different algorithms. However, the observed improvement is not as dramatic as seen in comparisons of A-scans. The reason can attribute to the factor of limited pixel rate in a captured image (512 pixels per 3mm), which can easily blur the differences.

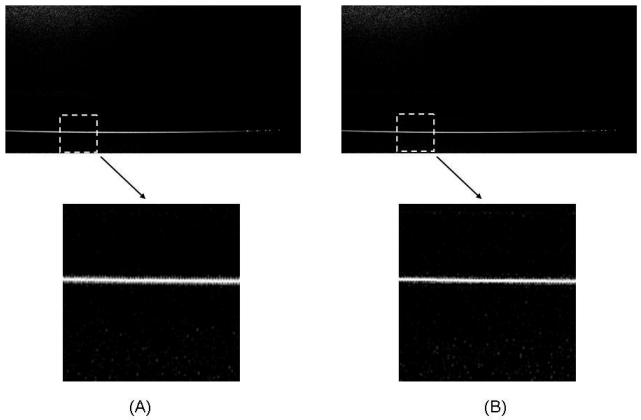

Fig. 4. Sample OCT images of the reflector at ~2.5mm depth, and corresponding local magnifications. Column (A): calibrated with regular clock; Column (B): calibrated with log-amplified clock.

#140944 - $15.00 USD Received 19 Jan 2011; revised 9 May 2011; accepted 25 May 2011; pub. 27 May 2011

4. Summary

Imprecise signal calibration with SS-OCT prevents optimal imaging of biological tissues such as coronary artery. In a SS-OCT, the calibration procedure of equidistantly redistributing the OCT signal into the frequency/wavenumber domain becomes essential for compensating any nonlinearity and instability during laser scanning. An auxiliary frequency clock, prevailingly based on an F-P interferometer or a Mach-Zehnder interferometer, can provide a form of frequency scale and therefore is popularly utilized for calibration. However, due to the nature of the clock signal generation and detection, phase errors and noises always present within the clock signal in reality. These distortions inevitably compromise the calibration accuracy, which ultimately hampers the system performance such as axial resolution and *SNR*. Although advanced calibration algorithms [17], based on sophisticated signal processing techniques, have demonstrated a prominent improvement, the considerable increment in computational burden might be a concern. The hardware-based approach presented here, which uses a true logarithmic amplifier to precondition the clock signal, provides a simple yet novel alternative to eliminate or suppress those distortions. Two mechanisms provide intrinsic merits over others. This approach was validated and tested with a high-speed SS-OCT and demonstrates superior ability on optimal calibration without burdening the computation time.

Acknowledgments

Dr. Brezinski's work is currently funded by National Institute of Health Grants R01 AR44812, R01 HL55686, R01 EB02638/HL63953, R01 AR46996 and R01 EB000419.

#140944 - $15.00 USD Received 19 Jan 2011; revised 9 May 2011; accepted 25 May 2011; pub. 27 May 2011